International Journal of Thermophysics, Vol. 22, No. 1, 2001

Nonequilibrium Molecular Dynamics Studies of Heat Flow in One-Dimensional Systems[1]

F. Zhang,[2,3] D. J. Isbister,[2] and D. J. Evans[4]

A nonequilibrium molecular dynamics (NEMD) heat flow algorithm is used to compute the heat conductivity of one-dimensional (1D) lattices. For the well-known Fermi–Pasta–Ulam (FPU) lattice, it is shown that for heat field strengths higher than a certain critical value, a stable solitary wave (soliton) can emerge spontaneously in molecular dynamics simulations. For lower field strengths the dynamics of the system are mostly chaotic; heat conductivity obtained via the NEMD algorithm increases monotonically with the size of the system. It is also demonstrated that the 1D nonequilibrium system may reach different steady states depending on the initial conditions.

KEY WORDS: molecular simulation; nonequilibrium system; statistical mechanics; solitary wave; thermal conductivity.

1. INTRODUCTION

Heat conduction in one-dimensional (1D) systems is a fundamental issue in statistical mechanics and has consequently attracted much interest. Surprisingly, it has been found that many 1D systems do not obey Fourier's law [1–19]. In fact, the thermal conductivity is divergent in the thermodynamic limit. For harmonically coupled oscillators, it was rigorously shown that the thermal conductivity λ is proportional to the number of oscillators N [1]. Such a divergence is founded in the existence of extended

[1] Paper presented at the Fourteenth Symposium on Thermophysical Properties, June 25–30, 2000 Boulder, Colorado, U.S.A.

[2] School of Physics, University College, ADFA (UNSW), Canberra, ACT 2612, Australia.

[3] To whom correspondence should be addressed.

[4] Research School of Chemistry, Australian National University, Canberra, ACT 0200, Australia.

0195-928X/01/0100-0135$19.50/0

waves (phonons) freely traveling (and carrying thermal energy) along the system without attenuation. In later studies [2, 3], impurities or defects in the chain were taken into account, since it was anticipated that phonon waves could be damped by the scattering processes due to such defects, thus possibly removing the N divergence of λ. However, it was demonstrated for isotopically disordered harmonic chains that the heat conductivity still diverged, albeit at a somewhat slower rate ($\lambda \approx N^{1/2}$) [2, 3]. Another way of trying to achieve normal heat conduction in 1D systems is by invoking anharmonicity [4], which makes the phonons interact among themselves, thus impeding their free propagation. However, Lepri et al. [12] have found that even strong nonlinearity and chaotic behavior are insufficient to ensure the existence of normal heat conduction. In the well-known Fermi–Pasta–Ulam (FPU) β model, they found a power-law divergence of the thermal conductivity $\lambda \propto N^{\gamma}$ for $\gamma \approx 0.4$. This power-law divergence was qualitatively attributed [13] to the long-time tail of the heat flux autocorrelation function, whose time integral gives the thermal conductivity of the system.

Many previous studies of heat conductivity have used a straightforward simulation method [6–17]. In molecular dynamics (MD) simulations two heat reservoirs with high and low temperatures, T_H and T_L, are located on each side of the system. The average heat flux and the internal temperature gradient are measured, with the thermal conductivity being the ratio of these two quantities. However, there are a number of disadvantages to this approach. In particular, the system is spatially inhomogeneous and one cannot define an intrinsic temperature T for the system due to the large temperature gradient acting across the system. Consequently, it is impossible to obtain the T dependence of the heat conductivity. In addition, problems associated with the use of the Nosé–Hoover thermostat for boundary particles have been identified and discussed in Ref. 15.

In this paper we present a detailed study of the Evans NEMD heat flow algorithm [20–22] for 1D systems. For sufficiently large heat fields, a stable well-defined solitary wave (soliton) can be generated spontaneously in simulations starting from random initial conditions. After the soliton is generated, the normal process of homogeneous heat conduction is destroyed, with the heat being transferred through the chain via the highly localized solitary wave. This results in a sharp increase in the effective thermal conductivity of the system. Due to this instability, progressively smaller fields are required, as the system size increases, to observe the linear regime of the thermal conductivity and thereby carry out the extrapolation of the thermal conductivity to zero field strength. Our simulation results also indicate that the heat conductivity increases with the size of the system, which is in qualitative agreement with previous findings [12–14].

2. NEMD EQUATIONS AND SOLITARY WAVES

We consider a 1D system of N particles located along the x axis. Each particle is allowed to move in the y direction, perpendicular to the x-axis, and we denote by q_i the displacement of the ith particle and by p_i the corresponding momentum. The Hamiltonian of the system is expressed as

$$\mathscr{H} = \sum_{i=1}^{N} \left[\frac{1}{2m} p_i^2 + U(q_{i+1} - q_i) \right] \tag{1}$$

where m is the particle's mass and U represents the interparticle interaction potential.

The Evans thermal conductivity algorithm for general systems of fluids has been described in detail [20–22]. The basis of this algorithm is the Green–Kubo relation for the thermal conductivity. For a 1D system defined by the Hamiltonian model (1), the thermal conductivity coefficient is given by [21]

$$\lambda = \lim_{\tau \to \infty} \frac{L}{k_B T^2} \int_0^{\tau} dt \langle J_x(t)\, J_x(0) \rangle_{eq} \tag{2}$$

where k_B is the Boltzmann constant, T is the absolute temperature of the system, and $L = Na$ is the system size. (The lattice constant a is taken to be unity in this paper.) The notation $\langle \cdots \rangle_{eq}$ denotes an equilibrium ensemble average. The heat flux vector, J_x, is given by

$$J_x(t) = -\frac{1}{2N} \sum \frac{p_i}{m} [\, U'(q_{i+1} - q_i) + U'(q_i - q_{i-1})] \tag{3}$$

In the Evans NEMD algorithm, the N-particle system is coupled to a "heat field" of strength f_e. The coupling is defined so that the energy dissipation is proportional to $J_x f_e$, i.e., $\mathrm{d}\mathscr{H}/\mathrm{d}t = L J_x f_e$, and that the condition of the adiabatic incompressibility of phase space (AIΓ) is satisfied [21]. The thermal conductivity coefficient can then be found from the ratio of the heat flux to the applied heat field in the infinite time and small field limit,

$$\lambda = \lim_{f_e \to 0} \lim_{t \to \infty} \frac{\langle J_x(t) \rangle}{T f_e} \tag{4}$$

Here $\langle J_x(t) \rangle$ is, in principle, a nonequilibrium ensemble average, but in practice, it is usually replaced by a time average of $J_x(t)$ if the nonequilibrium steady state is assumed to be unique. As pointed out in the literature

(e.g., Ref. 21), this heat flow algorithm is valid only in the linear regime, i.e., $|f_e| \to 0$. In the nonlinear regime of nonvanishing f_e, there is no known physical meaning or interpretation for the quantity, $\lim_{t\to\infty} \langle J_x(t)\rangle / T f_e$.

The equations of motion which satisfy the above conditions are

$$\dot{q}_i = p_i/m \tag{5}$$

$$\dot{p}_i = F_i + f_e D_i - \alpha p_i \tag{6}$$

where $F_i = U'(q_{i+1} - q_i) - U'(q_i - q_{i-1})$ is the total force on particle i due to the nearest neighbor interaction,

$$D_i = -\frac{1}{2}[U'(q_{i+1} - q_i) + U'(q_i - q_{i-1})] + \frac{1}{N}\sum_{j=1}^{N} U'(q_{j+1} - q_j) \tag{7}$$

and α is the thermostat multiplier. Either of the following two thermostats can be used:

$$\alpha_k = \frac{1}{2K_0}\sum_{j=1}^{N} \frac{p_j}{m}(F_j + f_e D_j) \tag{8}$$

$$\alpha_e = \frac{f_e}{2K_0}\sum_{j=1}^{N} \frac{p_j}{m} D_j \tag{9}$$

where $K_0 = \frac{1}{2}\sum_{j=1}^{N} p_j^2/m$. α_k and α_e are known as the constant-temperature and constant-energy thermostats, respectively.

For simplicity, we set $m = 1$. From Eqs. (5) and (6) we obtain

$$\ddot{q}_i = F_i + f_e D_i - \alpha \dot{q}_i \tag{10}$$

Introducing a new variable, $Q_i = q_i - q_{i-1}$, leads to

$$\ddot{Q}_i = U'(Q_{i+1}) - 2U'(Q_i) + U'(Q_{i-1}) - \tfrac{1}{2} f_e[U'(Q_{i+1}) - U'(Q_{i-1})] - \alpha \dot{Q}_i \tag{11}$$

Taking into account the cyclic boundary conditions of Eqs. (5) and (6), we find that the transformation $q_i - q_{i-1} = Q_i$, $i = 1, 2, \ldots, N$, has an inverse

$$\mathbf{q}(t) = \mathbf{B} \cdot \mathbf{Q}(t) \tag{12}$$

where $\mathbf{q}(t) = (q_1, q_2, \ldots, q_N)^T$ and $\mathbf{Q}(t) = (Q_1, Q_2, \ldots, Q_N)^T$ are column vectors, and $\mathbf{B}$ is an $N \times N$ matrix [19].

Substituting Eq. (12) into Eqs. (8) and (9), we obtain $\alpha \equiv \alpha(\mathbf{Q}, \dot{\mathbf{Q}})$ (subscripts are omitted). Inserting this expression for $\alpha(\mathbf{Q}, \dot{\mathbf{Q}})$ into Eq. (11)

yields a closed set of lattice dynamics equations for $\{Q_i(t), i=1,..., N\}$. Furthermore, we can seek solutions of the form $Q_i(t)=Q(i-Vt)\equiv Q(z)$ for traveling waves. Substituting this ansatz into Eq. (11), we obtain a nonlinear differential-delay equation,

$$V^2Q''(z)=U'(Q(z+1))-2U'(Q(z))+U'(Q(z-1)) \\ -\tfrac{1}{2}f_e[\,U'(Q(z+1))-U'(Q(z-1))\,]+\alpha(z)\,VQ'(z) \tag{13}$$

for all $z\in[0, N]$. Periodic boundary conditions require that $Q(0)=Q(N)$, and the condition $\sum_{i=1}^{N} Q_i(t)\equiv 0$ implies that

$$\int_0^N Q(z)dz\equiv 0 \tag{14}$$

If $f_e=\alpha=0$, the system simplifies to a 1D Hamiltonian lattice, and its corresponding differential–delay Eq. (13) may be solved analytically, at least for some nearest-neighbor interaction potentials, including the Toda potential [23] and the well-known FPU β model [18, 19, 24], where the interparticle interaction potential is $U(Q)=\frac{1}{2}Q^2+\frac{1}{4}\beta Q^4$. In the latter case, an approximate soliton solution takes the form $Q(x, t)=Q_s(x-Vt)+Q_0$ where,

$$Q_s(z)=\pm\sqrt{\frac{2(V^2-1)}{\beta}}\,\mathrm{sech}[\,2z\sqrt{(V^2-1)/V^2}\,] \tag{15}$$

$$Q_0=-\frac{1}{N}\int_{-N/2}^{N/2} Q_s(z)dz\approx\mp\frac{\pi V}{\sqrt{2\beta}\,N} \tag{16}$$

In the case $f_e\neq 0$ and $\alpha(z)\neq 0$, Eq. (13) cannot be solved analytically. A finite difference method and Newton's iteration method can be combined to obtain the soliton's configuration and velocity–amplitude relationship as a function of f_e. We have checked that the solitons are indeed solutions of the NEMD system by direct numerical simulations of Eqs. (5) and (6), with the soliton configuration being the initial values for (p_i, q_i). The solitons are very stable and travel in the system with a *preserved shape and velocity*. Furthermore, by initializing more than one soliton in the initial conditions, it is found that the system can support multiple solitons of equal velocity. (If their velocities are different, the faster solitons will catch up to the slower ones and consume them through interactions.) Thus, single or multiple solitons (of equal velocity) are steady states of this system for nonzero heat fields.

Furthermore, from Eq. (12) we have $\dot{\mathbf{q}}(t) = \mathbf{B} \cdot \dot{\mathbf{Q}}(t)$. Consequently, the contribution to the kinetic energy from the soliton can be estimated [18]

$$K_{sol} = \frac{1}{2} \sum_i \dot{q}_i^2 \approx \frac{1}{2} V^2 \int_{-\infty}^{\infty} Q_s^2(z)\, dz = \frac{V^3 \sqrt{V^2 - 1}}{\beta} \tag{17}$$

In numerical simulation we observe that when a soliton is generated, low amplitude phonon waves give a negligible contribution to the system's kinetic energy. In such a case, we have

$$\frac{V^3 \sqrt{V^2 - 1}}{\beta} = K_0 \equiv \frac{(N-2)\, T}{2} \tag{18}$$

where the Boltzmann constant k_B is set to unity. For any values of N and T, Eq. (18) has a unique solution $V > 1$, which is the (supersonic) speed of the solitary wave.

3. SIMULATION RESULTS

In applying the NEMD heat flow algorithm [Eqs. (5) and (6)] to the FPU β model, the parameter β is taken to be unity. Periodic boundary conditions are always used. The equations of motion are integrated using a fourth-order operator-splitting integrator [25]. Unless indicated otherwise, the initial conditions for q_i and p_i are always prepared in the following way: initial values for q_i and p_i are randomly assigned and then rescaled to fix the system's energy/temperature to its given initial value, with the total momentum and the center of mass of the system being zero (thus remaining so in the subsequent simulation). Then an equilibrium simulation ($f_e = 0$) is made for 10^6 time steps to reach a phase point in the associated equilibrium ensemble space. Once these initial conditions have been thus generated, the nonequilibrium simulation for a nonzero external field strength is generated for a time length of up to 10^5 units.

3.1. Constant-Temperature Thermostat

For a constant-temperature thermostat, we find that for a given temperature T and particle number N, stable solitary waves can be generated during simulations (which start from random initial conditions) *if* the heat field strength f_e is higher than a certain critical value $f_c(N)$, which is a decreasing function of the system size N. The solitary wave travels in the direction of heat flow (to the right in Fig. 1) with a supersonic speed ($V_s > 1$). After the soliton is generated, the normal process of homogeneous

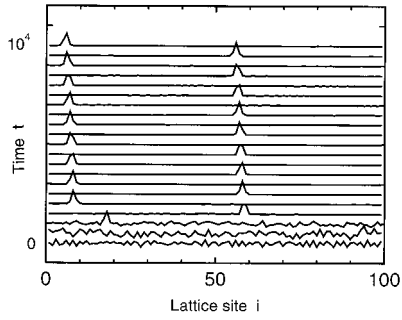

Fig. 1. The evolution of $Q_i(t) = q_{i+1}(t) - q_i(t)$, showing the generation of a solitary wave in the NEMD system. The heat field strength is $f_e = 0.006$, the system size is $N = 100$ particles, and the simulation temperature is $T \equiv 1$. Note that due to the periodic boundary conditions, the soliton enters into the left end of the lattice whenever it leaves the right end. Units are dimensionless for all figures.

heat conduction is destroyed and the heat flux increases dramatically (Fig. 2). In such a case, heat is transported in the form of a highly localized energy pulse carried by the soliton, and the average value of the heat flux is nearly independent of f_e.

It is found that the soliton's velocity increases with temperature and system size but is nearly independent of the heat field strength for $f_e \leqslant 1.0$. For example, for $N = 100$, $T = 10$, the soliton's velocity is found to be, 4.7, 4.7, and 4.8 for $f_e = 0.01$, 0.1, and 1.0, respectively. In addition, it is found that Eq. (18) gives very good estimates for the soliton's velocity. For instance, for $N = 100$, $T = 1$, Eq. (18) gives $V = 3.195$, and for $N = 200$, $T = 10$, $V = 4.709$; in the numerical simulations the soliton's velocity is found to be about 3.2 and 4.7 for these two cases, respectively.

When the heat field strength f_e is sufficiently low it is nearly impossible to generate a soliton from *random initial conditions*. In this case, the time-averaged heat flux $\langle J_x(t) \rangle$ can be measured and the conductivity, $\lim_{t \to \infty} \langle J_x(t) \rangle / (Tf_e)$, can be calculated. In Fig. 3 the heat conductivity obtained through the NEMD simulations is plotted. (Error bars are estimated to be within 10% at most.) The NEMD heat conductivity increases with the system size. When $f_e \to 0$ the conductivity converges to a finite value, which, according to the generalized Green–Kubo relation [21, 26], should equal the conductivity obtained through Eq. (2). We have

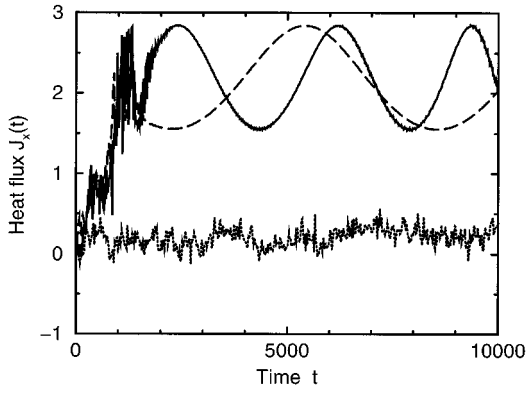

Fig. 2. The instantaneous heat flux in NEMD simulations of heat flow in the FPU model, with $f_e = 0.006$ (solid line) and $f_e = 0.01$ (dashed line), showing a drastic increase in heat flux when a soliton is generated about time $t = 1000$ in both cases. This is in contrast to the situation when no soliton is generated for $f_e = 0.002$ (dotted line). The parameters are $N = 100$ and $T \equiv 1$.

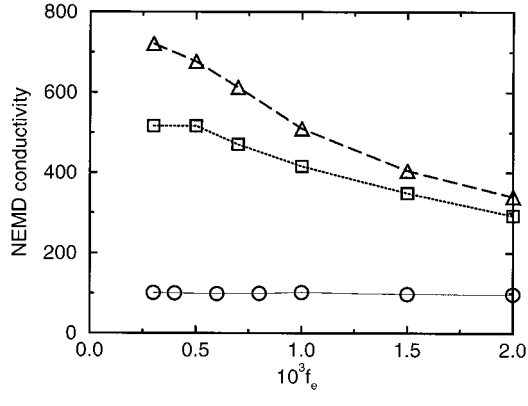

Fig. 3. The heat conductivity obtained from the NEMD simulation at $T \equiv 1$, for the FPU model with $N = 100$ (circles), 300 (squares), and 400 (triangles) particles.

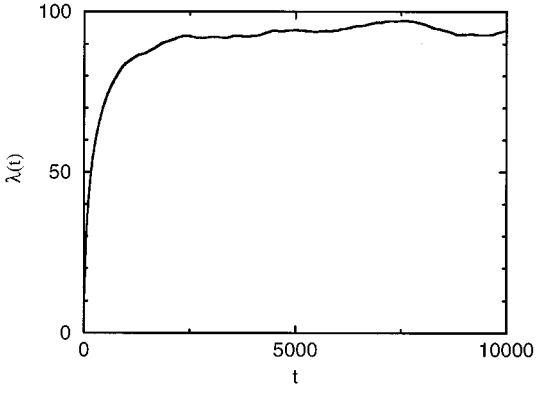

Fig. 4. The time-dependent heat conductivity $\lambda(t)$ calculated from the Green–Kubo formula, Eq. (19), for the FPU lattice with $N = 100$ particles and temperature $T \equiv 1$.

tested this convergence for the FPU system of $N = 100$ particles. In Fig. 4 we plot the function

$$\lambda(t) = \frac{N}{k_B T^2} \int_0^t d\tau \langle J_x(\tau)\, J_x(0) \rangle_{eq} \tag{19}$$

where the ensemble average is obtained by using 10 independent trajectories of length 10^6 units in time. It is clear that as $t \to \infty$, λ approaches a value around 93 (in reduced units), which is in good agreement with the heat conductivity obtained through NEMD algorithm. See Fig. 3.

3.2. Constant-Energy Thermostat

One of the most striking features to note is that for a given particle number N, and internal energy per particle, $E_p = \mathscr{H}/N$, the system dynamics depends on both the initial conditions and the field strength f_e and can be classified into two distinct types: spontaneous formation of a stable soliton and chaotic dynamics throughout the simulation (see Fig. 5). Moreover, we find that in every case once a soliton is generated it never dissipates but travels in the system for the entire length of the simulation run. This means that the transition from a chaotic to a soliton state is irreversible despite the equations of motion being time-reversible.

For a given field strength, there is a certain set of trajectories on which a soliton can emerge spontaneously. The probability of finding a soliton trajectory, denoted P_S, is plotted in Fig. 6 as a function of the field

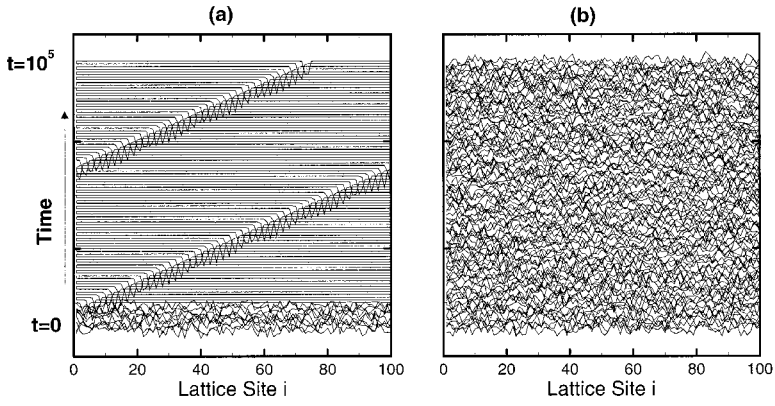

Fig. 5. The evolution of $Q_i(t)$ showing two types of steady state for the system with $f_e = 0.0045$, and $E_p = 1.0$, but different random initial conditions. (a) Spontaneous and irreversible formation of a soliton with a constant velocity $V_s \approx 2.9$; (b) chaos throughout the simulation. Note that a soliton's maximum amplitude can be either positive or negative.

strength. Here each data point is calculated from 20 sample trajectories which started from different random initial conditions. When f_e is very low the probability of generating a soliton is virtually zero, but the probability undergoes a sharp transition to unity over a critical region of the field strength.

The transient time to generate a soliton from the random initial conditions, denoted as T_S, depends strongly on both the initial conditions and

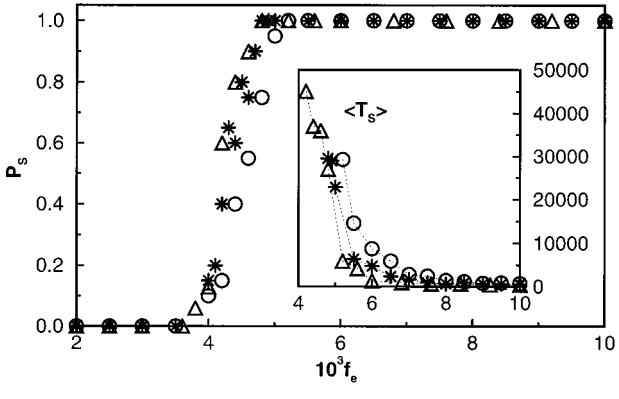

Fig. 6. The probability P_S and the average transient time $\langle T_S \rangle$ for soliton formation, as a function of the applied field strength f_e. The circles, stars, and triangles are for systems of 50, 100, and 200 particles, respectively.

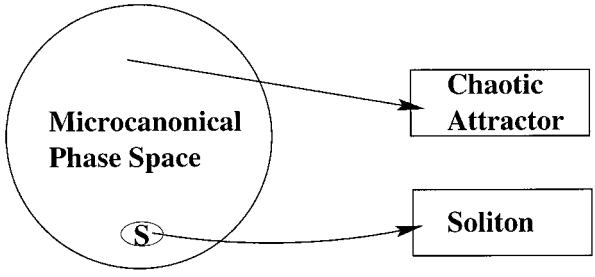

Fig. 7. Schematic illustration of the two steady states attained in the model system. The basin of attraction for the solitons is represented by the ellipse with a character **S** inside. It expands as f_e increases and becomes the whole microcanonical phase space once f_e is higher than a critical value.

the field strength. However, the ensemble average $\langle T_S \rangle$ is nearly constant for large fields and yet increases sharply as the field strength approaches the critical value f_c from the large field region. See Fig. 6.

This behavior remains qualitatively the same for different system size N and different average energy density E_p. In particular, for a fixed E_p, we find that the chaos–soliton transition becomes sharper as the system size is increased and that the critical field strengths $f_c(N)$ appear to approach a limiting value of $f_c \approx 0.0047$ for $N \geqslant 100$.

Based on these results, we can summarize the dynamics of this system as follows. For $f_e = 0$, the system is Hamiltonian (conservative); its dynamics are chaotic for *almost all* initial conditions, though it can support solitons for certain initial conditions (see Ref. 19 and references therein). For $f_e \neq 0$ the system is dissipative and its comoving phase space shrinks as time goes on. Some phase points collapse onto a strange chaotic attractor, and others, which are sufficiently close to the soliton solution of the corresponding Hamiltonian system, are attracted onto the soliton solution of the dissipative system. The basin of attraction for the soliton grows as f_e increases, until it eventually occupies the whole phase space when f_e is larger than a critical value (Figs. 6 and 7).

4. CONCLUDING REMARKS

In conclusion, we have shown that the Evans NEMD heat flow algorithm, which was designed originally for computing thermal conductivity in liquids, can generate solitons when applied to 1D systems. In the well-known FPU model, we have shown that when the heat field strength is higher than a critical value a stable soliton can be generated spontaneously

during simulations starting from random initial conditions. Because of this instability, sufficiently small fields have to be used to observe the linear regime of the thermal conductivity and thereby carry out the extrapolation to zero field to find the thermal conductivity's value. This poses an undesirable restriction on the algorithm for the computation of the thermal conductivity of 1D systems.

In addition, for constant-energy thermostated NEMD heat flow, we have demonstrated clearly that the nonequilibrium system may reach either a soliton-like steady state or a chaotic attractor, depending on the initial conditions. It should be stressed that such phenomena can be observed in many other NEMD models including 2D fluid particle systems [22] and 2D lattices. Further investigations are necessary to understand the implications of such multiple steady states for the computation of transport coefficients (such as thermal conductivities) and for nonequilibrium steady-state theories.

ACKNOWLEDGMENTS

We thank Professor E. G. D. Cohen for useful discussions. This work is supported by ARC Large Grant No. A69800064.

REFERENCES

1. Z. Rieder, J. L. Lebowitz, *J. Math. Phys.* **8**:1073 (1967).
2. H. Matsuda and K. Ishii, *Prog. Theor. Phys. Suppl.* **45**:56 (1970).
3. J. B. Keller, G. C. Papanicolaou, and J. Weilenmann, *Commun. Pure Appl. Math.* **32**:583 (1978).
4. R.E. Peierls, *Quantum Theory of Solids* (Oxford University Press, London, 1955).
5. F. Mokross and H. Buttner, *J. Phys. C* **16**:4539 (1983).
6. G. Casati, J. Ford, F. Vivaldi, and W. M. Visscher, *Phys. Rev. Lett.* **52**:1861 (1984).
7. M. Mareschal and A. Amellal, *Phys. Rev. A* **37**:2189 (1988).
8. E. A. Jackson and A. D. Mistriotis, *J. Phys. Condens. Matter* **1**:1223 (1989).
9. H. Kaburaki and M. Machida, *Phys. Lett. A* **181**:85 (1993).
10. A. Maeda and T. Munakata, *Phys. Rev. E* **52**, 234 (1995).
11. D. J. Mimnagh and L. E. Ballentine, *Phys. Rev. E* **56**:5332 (1997).
12. S. Lepri, R. Livi, and A. Politi, *Phys. Rev. Lett.* **78**:1896 (1997); *Physica D* **119**:140 (1998).
13. S. Lepri, R. Livi, and A. Politi, *Europhys. Lett.* **43**:271 (1998).
14. B. Hu, and B. Li, and H. Zhao, *Phys. Rev. E*, **57**:2992 (1998).
15. A. Fillipov, B. Hu, B.W. Li, and A. Zeltser, *J. Phys. A Math. Gen.* **31**:7719 (1998).
16. H. A. Posch, Wm. G. Hoover, *Phys. Rev. E* **58**:4344 (1998).
17. T. Hatano, *Phys. Rev. E* **59**:R1 (1999).
18. F. Zhang, D. J. Isbister, and D. J. Evans, *Phys. Rev. E* **61**:3541 (2000).
19. F. Zhang, D. J. Isbister, and D. J. Evans, submitted for publication.
20. D. J. Evans, *Phys. Lett. A* **91**:457 (1982).

21. D. J. Evans and G. P. Morriss, *Statistical Mechanics of Nonequilibrium Liquids* (Academic, New York, 1990).
22. D. J. Evans and H. J. M. Hanley, *Mol. Phys.* **68**:97 (1989); D. P. Hansen and D. J. Evans, *Mol. Phys.* **81**:767 (1994); D. P. Hansen and D. J. Evans, *Mol. Sim.* **14**:409 (1995).
23. M. Toda, *Theory of Nonlinear Lattices* (Springer-Verlag, Berlin, 1981).
24. J. A. D. Wattis, *J. Phys. A Math. Gen* **26**:1193 (1993).
25. F. Zhang, *J. Chem. Phys.* **106**:6102 (1997).
26. S. Sarman, D. J. Evans, and P. T. Cummings, *Phys. Rep.* **305**:1 (1998).